Journal of Materials Chemistry A

PAPER

View Article Online
View Journal | View Issue

Published on 20 February 2017. Downloaded by Synchrotron Radiation Library on 12/12/2017 06:48:23.

Cite this: J. Mater. Chem. A, 2017, 5, 11739

High efficiency ternary organic solar cell with morphology-compatible polymers†

Jiangquan Mai,[a] Haipeng Lu,[b] Tsz-Ki Lau,[a] Shih-Hao Peng,[c] Chain-Shu Hsu,[c] Wenqiang Hua,[d] Ni Zhao,[b] Xudong Xiao[a] and Xinhui Lu*[a]

Received 10th January 2017
Accepted 18th February 2017

DOI: 10.1039/c7ta00292k

rsc.li/materials-a

Ternary organic solar cell is a promising strategy for improving the power conversion efficiency (PCE) of single-junction organic solar cells by broadening the light absorption spectrum with the incorporation of two electron donors and one acceptor or one donor and two acceptors. However, in many cases the optimized loading of the third component is so small that its contribution to the light absorption is limited. Following our previously proposed selection rule for the two polymers capable of comparable loadings, we report in this work a ternary system composed of two morphologically compatible polymers with distinct chemical structures that can achieve a high PCE of 9.0% with a mass ratio of 1 : 1. Besides the expected improvement in short circuit current due to the broadening of the absorption spectrum, the fill factor of the ternary device is improved significantly. We attribute it to the balanced electron and hole mobility and reduced recombination benefiting from the high morphology compatibility of the system.

Introduction

Organic photovoltaic (OPV) devices have recently attracted increasing attention as a low cost alternative to silicon based solar cells due to the unique advantages such as lightweight, semitransparent, flexible, solution processible and capable of large scale roll-to-roll manufacturing. By developing new materials and morphology controls,[1–3] the record efficiency has been broken through repeatedly (current record = 11.7%),[3] approaching the theoretical limit of single-junction binary cells.[4] To overcome this limitation, tandem and ternary solar cells are fabricated to broaden the absorption range by involving two major light absorbers[5,6] with complementary absorption spectra. Unlike tandem organic solar cells, which require complex multi-junctions in device fabrication, ternary solar cells simply mix two donors with one acceptor or one donor with two acceptors together to form one single bulk heterojunction active layer, offering a more cost-effective route for further improving the PCE of organic solar cells. Many successful ternary systems with enhanced light absorption and efficiency are reported recently.[7–10] However, the morphology control becomes even more challenging for ternary systems since one are dealing with a three-component intermixing problem. Many ternary systems cannot incorporate comparable loadings of each component,[11–13] which largely reduces the absorption benefits of employing an additional light absorber. There are very limited studies reported so far to address this problem. Similar chemical structures and surface energy were suggested to be the key factors for polymers being able to work with comparable loadings.[14,15] Tunable open circuit voltage with different polymer mass ratios was proposed to be an indicator of a compatible ternary system.[15–17] Besides, Yang reported several benzodithiophene-based polymers which are able to have similar molecular orientation, crystallinity and domain size, showing high structural compatibility and an improved performance.[18] In contrast, our recent work suggested that morphology compatibility is a prerequisite criteria for selecting two compatible polymers.[19] We found that polymers that have strong lamellar interactions and similar phase separation behavior with fullerene derivatives are more likely to be able to work with comparable loadings in a ternary system. Interestingly, the device performance improvement observed in compatible ternary system is not only reflected by the enhancement of short circuit current density (J_{sc}) but also fill factor (FF), which is yet to be understood for further improving the PCE of ternary solar cell.

In the present work, following the selection rule proposed in ref. 19, we employed poly[4,8-bis(5-(2-ethylhexyl)thiophen-2-yl) benzo[1,2-*b*:4,5-*b*′]dithiophene-*co*-3-fluorothieno[3,4-*b*]thiophene-2-carboxylate] (PTB7-Th) and poly(5,6-difluorobenzothiadiazole-*alt*-quaterthiophene) containing porphyrin side

[a]Department of Physics, The Chinese University of Hong Kong, New Territories, Hong Kong, China. E-mail: xhlu@phy.cuhk.edu.hk
[b]Department of Electronic Engineering, The Chinese University of Hong Kong, New Territories, Hong Kong, China
[c]Department of Applied Chemistry, National Chiao Tung University, Hsinchu, Taiwan
[d]Shanghai Synchrotron Radiation Facility, 239 Zhangheng Road, Pudong New District, Shanghai, China

† Electronic supplementary information (ESI) available. See DOI: 10.1039/c7ta00292k

Published on 20 February 2017. Downloaded by Synchrotron Radiation Library on 12/12/2017 06:48:23.

groups (PPor-2) as major light absorbers and electron donors, and [6,6]-phenyl-C_{71}-butyric acid methyl ester ($PC_{71}BM$) as an electron acceptor to form a ternary system. Grazing incidence wide/small-angle X-ray scattering (GIWAXS/GISAXS) measurements confirmed that these two polymers are morphologically compatible even with totally different chemical structures. In agreement with the morphology results, the best device performance was achieved at the PTB7-Th : PPor-2 mass ratio of 1 : 1 for this ternary system. Besides the expected improvement in J_{sc} due to the broadening of the absorption spectrum, the FF of the ternary device was improved significantly. We investigated the charge transport properties and found that the ternary hole and electron mobility tended to adopt the relatively higher values of the corresponding mobility in binary cells, because of the high morphology compatibility. In addition, more efficient charge dissociation and reduced recombination were observed. This work provides further evidences of the importance of morphology compatibility in ternary organic solar cell and insights on understanding on the improved photovoltaic process of compatible ternary systems.

Experimental section

Materials

PTB7-Th was purchased from Lumtech, $PC_{71}BM$ from American Dye Source. PPor-2 was synthesized by Prof. Chain-shu Hsu's research group.[20] All these materials are used as received without any modification or purification.

Device fabrication

The two polymers and $PC_{71}BM$ were separately dissolved in *ortho*-dichlorobenzene (DCB) with 3% diiodooctane additive and mixed as binary solutions (PTB7-Th : $PC_{71}BM$ (1 : 1.5) 25 mg ml^{-1}, PPor-2 : $PC_{71}BM$ (1 : 2) 30 mg ml^{-1}). Then binary solutions are mixed according to designed polymer mass ratios to form ternary solutions. ITO substrates were cleaned stepwise with deionized water, acetone and isopropanol in ultrasonic cleaner for 20 min and then treated with oxygen plasma. PEDOT:PSS layer was spun coated on the cleaned ITO substrates with a spin speed of 4000 rpm and then annealed under 130 °C for 20 min in glove box. Active layers were spun coated on the top of PEDOT:PSS and the thicknesses are controlled by spin speed. With above binary solutions, ~110 nm active layers were achieved with 1500 rpm, and their ternary mixture solutions of different mass ratios could all achieve the similar thicknesses of ~110 nm with the same spin speed. After the active layers were dried in nitrogen atmosphere for 30 min, methanol treatment[21] was performed. Next, 10 nm Ca and 100 nm Al are evaporated onto the active layer under a vacuum of 7×10^{-4} Pa. The effective area of the device is 0.03 cm^2.

Characterization method

The solar cell performance was measured by a Keithley 2612 source meter unit under an AM 1.5G solar simulator with an intensity of 100 mW cm^{-2}. UV-Vis absorption spectra were taken on a Cary 5G UV-Vis-NIR spectrophotometer.

The GIWAXS measurements were conducted at 23A SWAXS beamline at the National Synchrotron Radiation Research Center, Hsinchu, Taiwan, using a 10 keV primary beam, 0.15° incident angle and C9728DK area detector.[22] The GISAXS measurements are conducted at 19U2 beamline at Shanghai Synchrotron Radiation Facility, Shanghai, China with 12 keV primary beam, 0.15° incidence angle and Pilatus 1M-F detector. Both GIWAXS and GISAXS samples are prepared on PEDOT:PSS coated silicon substrate by spin coating.

Results and discussion

Polymer compatibility

In our previous study about the morphology compatibility of ternary solar cells,[19] despite of different chemical structures and overlapping absorption spectra, PTB7 and PPor-2 was identified to be highly compatible in morphology based on the best performing ternary cells (mass ratio = 1 : 1) compared to the binary cells (ESI Fig. S1a†). In order to take advantage of the light absorption compensation, here we replaced PTB7 with PTB7-Th, which shows a relatively redshift absorption edge up to around 800 nm, to be complementary with the absorption range of PPor-2 (Fig. S1b†). Fig. 1d shows the UV-Vis absorption spectra of PTB7-Th:$PC_{71}BM$, PPor-2:$PC_{71}BM$ and the ternary blend film. The ternary PTB7-Th : PPor-2(1 : 1):$PC_{71}BM$ film adopts both the red-shifting absorption edge of PTB7-Th at ~800 nm and a large range absorption enhancement between 350 nm and 700 nm contributed from PPor-2. As shown in Fig. 1c, the energy levels of PTB7-Th lie in the middle of those of PPor-2, so this ternary system follows the parallel-like charge transfer mechanism[5,23,24] where charge transfer mainly occurs between PTB7-Th and $PC_{71}BM$ or PPor-2 and $PC_{71}BM$. Therefore the electron trapping at PTB7-Th:PPor-2 interface can be neglected.

The morphology of the ternary and binary films was investigated by GIWAXS and GISAXS, which offer the molecular level and nanoscale structural information of the active layer respectively.[11,19,25,26] Fig. 2a–c present the two-dimensional GIWAXS patterns of PTB7-Th:$PC_{71}BM$, PPor-2:$PC_{71}BM$ binary films and the PTB7-Th : PPor-2(1 : 1):$PC_{71}BM$ ternary film. The PTB7-Th:$PC_{71}BM$ blend film (Fig. 2a) showed weakly face-on orientational preference with an almost ring-like lamellar peak at $q \approx 0.305$ $Å^{-1}$ (lattice spacing $d \approx 20.6$ Å), concentrated slightly along q_r axis and a weak and broad π–π peak appeared in the out-of-plane direction at $q_z \approx 1.60$ $Å^{-1}$ ($d \approx 3.93$ Å), partially overlapping with the amorphous $PC_{71}BM$ ring ($q \approx 1.37$ $Å^{-1}$). In contrast, the PPor-2:$PC_{71}BM$ blend film (Fig. 2c) presented a strong edge-on oriented packing with strong and definite lamellar and π–π peaks appeared at $q_z \approx 0.385$ $Å^{-1}$ ($d \approx 16.3$ Å) and $q_r \approx 1.77$ $Å^{-1}$ ($d \approx 3.54$ Å), respectively. For the PTB7-Th : PPor-2(1 : 1):$PC_{71}BM$ blend film (Fig. 2b), only one ring-like lamellar peak was observed at $q \approx 0.329$ $Å^{-1}$, in between the lamellar peak positions of both binary films. This unifying of lamellar peak in ternary film is an evidence of strong lamellar interaction between the two donor polymers, a signature of high morphology compatibility.[16,19]

 This journal is © The Royal Society of Chemistry 2017

Published on 20 February 2017. Downloaded by Synchrotron Radiation Library on 12/12/2017 06:48:23.

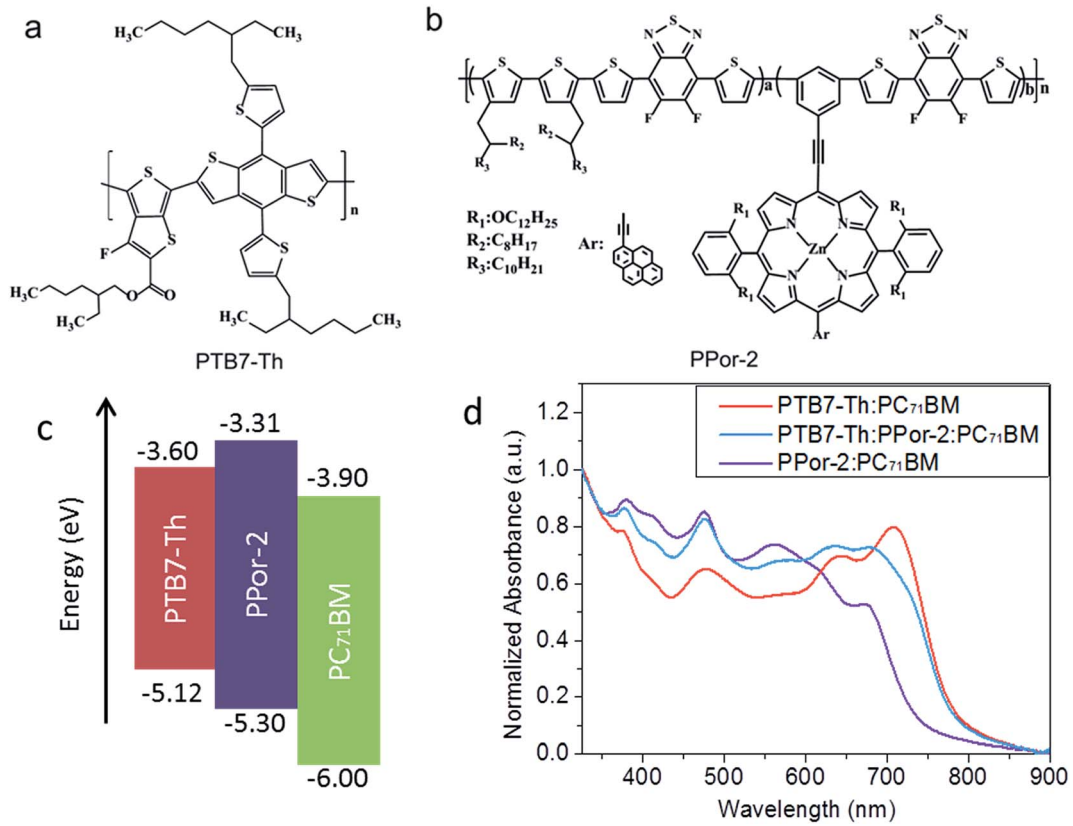

Fig. 1 Chemical structures of (a) PTB7-Th and (b) PPor-2; (c) energy level alignment of materials used in the active layer; (d) UV-Vis absorption spectra of PTB7-Th:$PC_{71}BM$, PPor-2:$PC_{71}BM$ and PTB7-Th : PPor-2(1 : 1):$PC_{71}BM$ blend films.

The in-plane nanoscale phase separation information was investigated by GISAXS *via* effective surface approximation.[27] Fig. 2d–f show GISAXS patterns and Fig. 2h shows the intensity profiles in the q_r direction at the reflected beam position. To quantify the domain sizes of each phase, the GISAXS profiles were fitted with the Debye–Anderson–Brumberger (DAB) model for amorphous phases with dispersed $PC_{71}BM$ molecules and the fractal-like network model for aggregated $PC_{71}BM$ clusters.[2,19,28] Although the small-angle scattering contributions from crystalline PTB7-Th and PPor-2 domains are neglected due to the lack of contrast, we can roughly estimate the size of "alloyed" polymer crystalline domains from the correlation length of the lamella stacking obtained from the ternary GIWAXS pattern using Scherrer equation (Fig. 2g). The fitting results are shown in Table S1.† For the ternary solar cell, the domain sizes of amorphous phase ξ, clustered $PC_{71}BM$ phase $2R_{gPC_{71}BM}$ and polymer phases $L_{polymer}$ are around 8 nm, 60 nm and 5 nm respectively. The fitted fractal dimension (D) which corresponds to the packing density of $PC_{71}BM$ clusters is 1.87 for the PPor-2:$PC_{71}BM$ binary film, 2.09 for PTB7-Th:$PC_{71}BM$ film and 2.13 for the ternary film, consistent with the similar fullerene packing density signature of compatible system.[19] In addition, atomic force microscope (AFM) measurement was also conducted and the results are shown in Fig. S2.† Both binary films and ternary film show similar top-surface morphology in the AFM images, indicating similar phase separation behaviors consistent with the GISAXS results. In summary, PPor-2 and PTB7-Th have demonstrated good morphology compatibility.

Device photovoltaic characterization

The ternary PTB7-Th:PPor-2:$PC_{71}BM$ solar cells and their binary devices are fabricated with the conventional structure of ITO/PEDOT:PSS/active layer/Ca/Al to demonstrate their photovoltaic performance. For the binary control devices, the mass ratios of PTB7-Th : $PC_{71}BM$ and PPor-2:$PC_{71}BM$ are kept to 1 : 1.5 and 1 : 2, respectively as optimized in previous studies.[20,29,30] So in the ternary solar cell, the polymer fullerene mass ratio is kept as PTB7-Th : PPor-2 : $PC_{71}BM$ = A : B : (1.5A + 2B). The photovoltaic performance of all devices are measured under AM 1.5G solar illumination. Current density *versus* applied voltage (J–V) curves and external quantum efficiency (EQE) curves of the ternary system are shown in Fig. 3a and b, and the characteristic parameters are summarized in Table 1. The optimized mass ratio of PTB7-Th : PPor-2 in the ternary system turns out to be 1 : 1, in agreement with their high morphology compatibility. At this mass ratio, the ternary solar cell can achieve an average PCE of 9.0% outperforming both binary control cells (8.1% for PTB7-Th:PC_{71}-BM and 5.1% for PPor-2:$PC_{71}BM$). The performance enhancement is reflected in both short circuit current density (J_{sc}) and fill factor (FF). The J_{sc} of ternary solar cell has reached 16.9 mA cm^{-2}, making 9.7% improvement comparing with the J_{sc} of PTB7-Th:$PC_{71}BM$ binary cells (15.4 mA cm^{-2}). As shown in Fig. 3b, the

Published on 20 February 2017. Downloaded by Synchrotron Radiation Library on 12/12/2017 06:48:23.

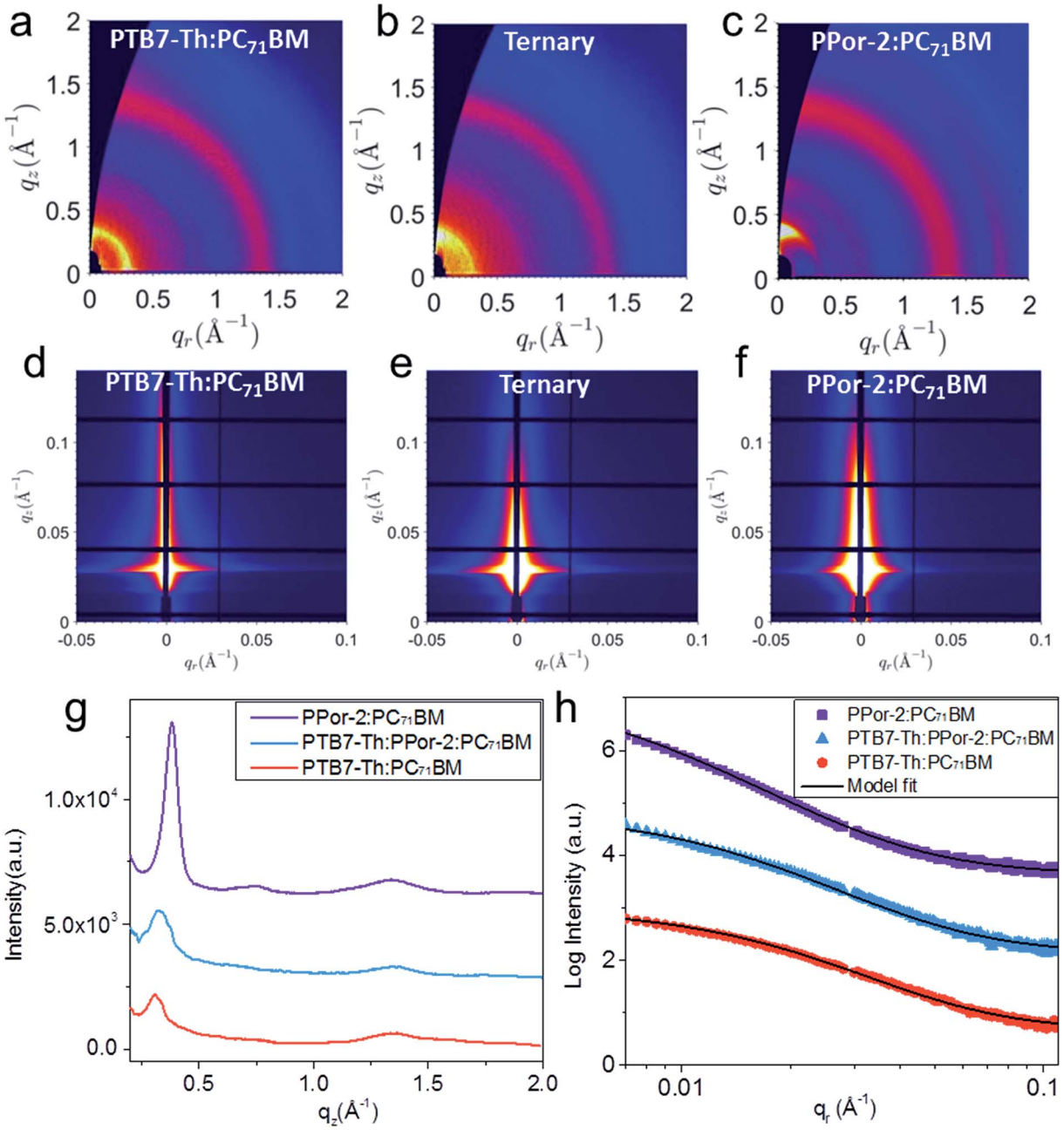

Fig. 2 GIWAXS patterns of (a) PTB7-Th:$PC_{71}BM$, (b) PTB7-Th : PPor-2(1 : 1):$PC_{71}BM$ and (c) PPor-2:$PC_{71}BM$; GISAXS patterns of (d) PTB7-Th:$PC_{71}BM$, (e) PTB7-Th:PPor-2(1 : 1):$PC_{71}BM$ and (f) PPor-2:$PC_{71}BM$; (g) GIWAXS intensity profiles along q_z axis; (h) GISAXS intensity profiles along q_r axis.

ternary solar cell (PTB7-Th : PPor-2 = 1 : 1) have a broad EQE increase between ~300 nm and ~700 nm compared with that of PTB7-Th binary cell, which is consistent with the absorption enhancement of ternary film from the PTB7-Th binary film (Fig. 1d). The J_{sc} calculated from EQE integration is 16.4 mA cm^{-2}, in good agreement with the measured J_{sc} (16.9 mA cm^{-2}, the error <3%). In particular, the absorption peak around 480 nm in PPor-2 showed important contribution in the EQE improvement of ternary solar cells. More interestingly, this ternary combination presented a significant FF enhancement from 0.64 and 0.61 for both binary controls to 0.69 at the optimized mass ratio (1 : 1) (Table 1). From the view of parasitic resistances, we found that the best ternary mass ratio showed the smallest series resistance and the largest shunt resistance among other controls, indicating that the high morphology compatibility of this ternary system could also gave rise to a high-quality bulk heterojunction film capable of efficient charge transfer and collection in addition to the absorption enhancement.

Charge dissociation, transport and recombination dynamics

To understand the light absorption and charge extraction properties of the ternary solar cells, we measured the

 This journal is © The Royal Society of Chemistry 2017

Published on 20 February 2017. Downloaded by Synchrotron Radiation Library on 12/12/2017 06:48:23.

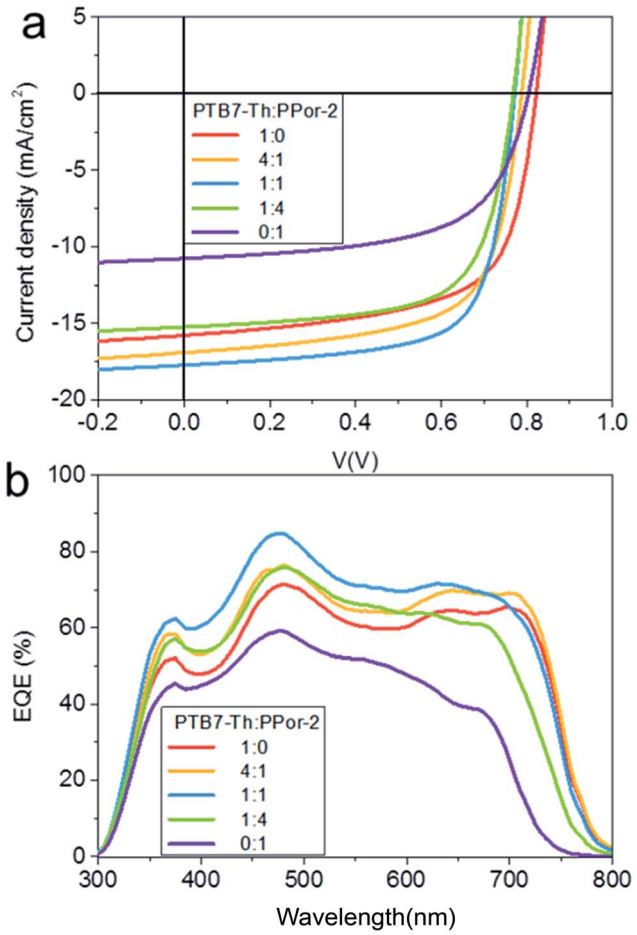

Fig. 3 (a) J–V curve of ternary solar cells with different polymer mass ratios; (b) external quantum efficiency of ternary solar cells with different polymer mass ratios.

photocurrent density (J_{ph}) *versus* the effective voltage (V_{eff}) of the ternary cells and their binary control cells (Fig. 4a).[2,24] J_{ph} is defined as $J_{ph} = J_L - J_D$, where J_L and J_D is the current density under illumination and the dark. And V_{eff} is defined as $V_{eff} = V_0 - V_{bias}$, where V_0 is the voltage when photocurrent is equal to zero and V_{bias} is the external applied voltage bias. Thus V_{eff} determines the electric field in the BHJ that affects the charge dissociation and transport process. At a high V_{eff}, the photogenerated free carriers are driven to move rapidly to the electrode and recombination loss is minimized, the saturated photocurrent J_{sat} is only limited by incident photon absorption. In Fig. 4a, at a high V_{eff} ($V_{eff} = 3$ V), the J_{sat} values for the three devices are 17.3 mA cm^{-2} (PTB7-Th:$PC_{71}BM$), 18.6 mA cm^{-2} (PTB7-Th:PPor-2:$PC_{71}BM$) and 11.9 mA cm^{-2} (PPor-2:$PC_{71}BM$). Thus compared with PTB7-Th:$PC_{71}BM$ binary cells, J_{sat} in ternary solar cell has an improvement of 7.5% which mainly attributes to the enhancement of light absorption. However this percentage of improvement is still not enough to account for the overall J_{sc} improvement of 9.7%, indicating that there should be some other effects contributing to the J_{sc} improvement. The charge dissociation possibilities under short circuit condition can be calculated by the ratio of J_{sc} and J_{sat} (J_{sc}/J_{sat}),[24,31] which are 89% for PTB7-Th:$PC_{71}BM$, 91% for PTB7-Th:PPor-2:$PC_{71}BM$, and 89% for PPor-2:$PC_{71}BM$. Therefore, the ternary solar cells have not only enhanced light absorption but also efficient charge dissociation, owning to the highly compatible morphology.

To investigate the charge collection properties, hole and electron mobilities of the ternary devices and their binary controls are measured by space charge limited current method[32,33] with hole-only and electron-only device. The device architecture is ITO/PEDOT:PSS/active layer/MoO_3/Au for the hole-only device and ITO/ZnO/active layer/Ca/Al for the electron-only device. The J–V curves are presented in Fig. 4b and c and fitted with Mott–Gurney law (eqn (1)), where J is current density, ε is the relative dielectric constant of the active layer, ε_0 is the permittivity of free space, μ is the carrier mobility, L is the thickness of active layer and V is the effective applied voltage on the active layer.

$$J = \frac{9}{8}\varepsilon\varepsilon_0\mu\frac{V^2}{L^3} \quad (1)$$

Both hole mobility and electron mobility results are summarized in Table 2. The hole mobility of PTB7-Th:$PC_{71}BM$ binary film (4.1×10^{-4} cm^2 V^{-1} s^{-1}), is higher than that of PPor-2:$PC_{71}BM$ binary film (1.6×10^{-4} cm^2 V^{-1} s^{-1}). In contrast, the electron mobility, PPor-2:$PC_{71}BM$ (8.6×10^{-4} cm^2 V^{-1} s^{-1}) is higher than PTB7:$PC_{71}BM$ (3.6×10^{-4} cm^2 V^{-1} s^{-1}). For the ternary film, it seems to be able to adopt the relatively higher hole (4.7×10^{-4} cm^2 V^{-1} s^{-1}) and electron (8.9×10^{-4} cm^2 V^{-1} s^{-1}) mobilities from the binary controls. Higher carrier mobility can reduce the series resistance by increasing the conductivity of the active layer,[34] therefore partially contributing to the observed FF enhancement.

To further understand the recombination dynamics, we measured the transient photovoltage (TPV) and transient

Table 1 Photovoltaic characteristics of binary and ternary solar cells[a]

Sample	J_{sc} (mA cm^{-2})	V_{oc} (V)	FF	PCE (%)	R_s (Ω)	R_{sh} (Ω)
PTB7-Th:$PC_{71}BM$	15.4 ± 0.3	0.82 ± 0.01	0.64 ± 0.01	8.1 ± 0.1	4.26 ± 0.24	436 ± 21
PTB7-Th : PPor-2(4 : 1):$PC_{71}BM$	16.5 ± 0.4	0.79 ± 0.01	0.66 ± 0.01	8.7 ± 0.2	3.88 ± 0.14	604 ± 51
PTB7-Th : PPor-2(1 : 1):$PC_{71}BM$	16.9 ± 0.5	0.77 ± 0.01	0.69 ± 0.01	9.0 ± 0.2	3.77 ± 0.26	918 ± 87
PTB7-Th : PPor-2(1 : 4):$PC_{71}BM$	14.9 ± 0.5	0.77 ± 0.01	0.67 ± 0.01	7.7 ± 0.3	4.61 ± 0.27	819 ± 81
PPor-2:$PC_{71}BM$	10.6 ± 0.3	0.80 ± 0.01	0.61 ± 0.01	5.1 ± 0.1	8.60 ± 0.57	741 ± 31

[a] The statistics in this table are based on 12 individual devices.

Published on 20 February 2017. Downloaded by Synchrotron Radiation Library on 12/12/2017 06:48:23.

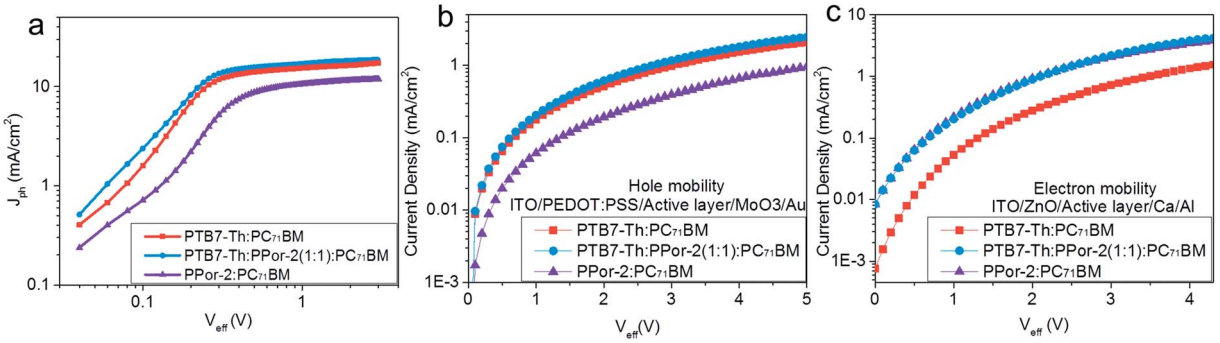

Fig. 4 (a) Photocurrent *versus* effective voltage characteristics; (b) *J*–*V* curve of hole-only devices for hole mobility measurement; (c) *J*–*V* curve of electron-only devices for electron mobility measurement.

Table 2 Hole and electron mobilities for ternary solar cells and their binary controls

	Hole mobility ($\times 10^{-4}$ cm^2 V^{-1} s^{-1})	Electron mobility ($\times 10^{-4}$ cm^2 V^{-1} s^{-1})
PTB7-Th:PC$_{71}$BM	4.1 ± 0.2	3.6 ± 0.2
PTB7-Th : PPor-2(1 : 1):PC$_{71}$BM	4.7 ± 0.6	8.9 ± 0.7
PPor-2:PC$_{71}$BM	1.6 ± 0.3	8.6 ± 0.7

photocurrent (TPC) on the ternary cells and their binary control with the method reported in ref. 33. Applying a pulse laser light to perform the TPV measurement, we can extract the carrier lifetime (τ) under different open circuit voltage (V_{oc}) controlled by varying the background light intensity from 0.01 to 1.0 sun. We then measured TPC using the same laser intensity to extract the carrier density (n) under different V_{oc}s. It is found that the best ternary solar cell has the highest carrier density, consistent with the observed highest J_{sc} (Fig. S4b†). Combining the results of TPV and TPC, we can obtain the relationship between carrier lifetime (τ) and carrier density (n) (Fig. 5a). We found that under the same carrier density, carrier lifetime in the ternary solar cell is much longer than both binary control solar cells. Fig. 5b shows the bimolecular recombination rate constants k, which can be calculated by $k = \frac{1}{(\lambda+1)n\tau(n)}$, where λ is an constant extracted from Fig. 5a with $\tau = \tau_0 n^{-\lambda}$. The results suggested that under the same carrier density, PPor-2:PC$_{71}$BM have a smaller carrier recombination rate than that of PTB7-Th:PC$_{71}$BM, and after forming the ternary film the recombination rate is further reduced. This result is correlated with the increased shunt resistance in the ternary solar cell which also contributes to the improved FF.

Conclusion

In summary, a high performance ternary system PTB7-Th:PPor-2:PC$_{71}$BM has been demonstrated with significant enhancement in J_{sc} and FF, compared to both of the binary controls. The two donor polymers are identified to be highly compatible in morphology with strong lamellar interaction and similar fullerene packing density. As a consequence, the optimized polymer mass ratio is 1 : 1, which achieved a high PCE over 9.0%. The enhancement in J_{sc} is not only attributed to the broadening of light absorption spectrum, but also more efficient charge dissociation. Moreover, the increase of FF is assigned to the contributions from higher and more balanced

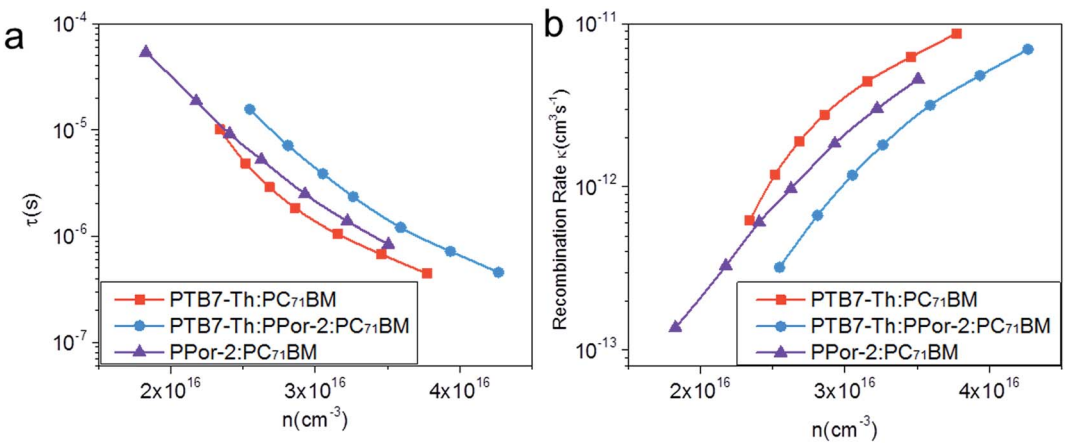

Fig. 5 (a) Life time of carriers *versus* carrier density; (b) recombination rate *versus* carrier density.

 This journal is © The Royal Society of Chemistry 2017

Published on 20 February 2017. Downloaded by Synchrotron Radiation Library on 12/12/2017 06:48:23.

charge carrier mobilities selectively adopted from the binary cells and reduced charge recombination. It is suggested that when selecting candidate polymers for a ternary solar cell, besides the absorption spectrum matching, morphology compatibility should be another important factor to consider. It not only allows the comparable loadings of the two polymers to maximize the absorption enhancement, but also largely benefits the charge dissociation and collection properties as well as suppressing the unwanted recombination.

Acknowledgements

We gratefully thank the beam time and technical supports provided by 23A SWAXS beamline at NSRRC, Hsinchu and 14B1, 16B1 and 19U2 beamlines at SSRF, Shanghai. We acknowledge the financial support from Research Grant Council of Hong Kong (General Research Fund No. 2130394 and Theme-based Research Scheme No. T23-407/13-N).

References

1 Y. Liu, J. Zhao, Z. Li, C. Mu, W. Ma, H. Hu, K. Jiang, H. Lin, H. Ade and H. Yan, *Nat. Commun.*, 2014, **5**, 5293.
2 Y. Lin, Q. He, F. Zhao, L. Huo, J. Mai, X. Lu, C. J. Su, T. Li, J. Wang, J. Zhu, Y. Sun, C. Wang and X. Zhan, *J. Am. Chem. Soc.*, 2016, **138**, 2973–2976.
3 J. Zhao, Y. Li, G. Yang, K. Jiang, H. Lin, H. Ade, W. Ma and H. Yan, *Nat. Energy*, 2016, **1**, 15027.
4 K. M. Coakley and M. D. McGehee, *Chem. Mater.*, 2004, **16**, 4533–4542.
5 A. Tayebeh, K. Parisa, M. Jie and J. B. Christoph, *Adv. Mater.*, 2013, **25**, 4245–4266.
6 T. Ameri, N. Li and C. J. Brabec, *Energy Environ. Sci.*, 2013, **6**, 2390–2413.
7 P. P. Khlyabich, B. Burkhart and B. C. Thompson, *J. Am. Chem. Soc.*, 2012, **134**, 9074–9077.
8 L. Yang, H. Zhou, S. C. Price and W. You, *J. Am. Chem. Soc.*, 2012, **134**, 5432–5435.
9 T. Ameri, J. Min, N. Li, F. Machui, D. Baran, M. Forster, K. J. Schottler, D. Dolfen, U. Scherf and C. J. Brabec, *Adv. Energy Mater.*, 2012, **2**, 1198–1202.
10 Q. An, F. Zhang, J. Zhang, W. Tang, Z. Deng and B. Hu, *Energy Environ. Sci.*, 2016, **9**, 281–322.
11 J. Q. Mai, T. K. Lau, T. Xiao, C. J. Su, U. S. Jeng, N. Zhao, X. D. Xiao and X. H. Lu, *RSC Adv.*, 2015, **5**, 88500–88507.
12 S. Liu, P. You, J. Li, J. Li, C.-S. Lee, B. S. Ong, C. Surya and F. Yan, *Energy Environ. Sci.*, 2015, **8**, 1463–1470.
13 M. C. Chen, D. J. Liaw, Y. C. Huang, H. Y. Wu and Y. Tai, *Sol. Energy Mater. Sol. Cells*, 2011, **95**, 2621–2627.
14 P. P. Khlyabich, A. E. Rudenko, R. A. Street and B. C. Thompson, *ACS Appl. Mater. Interfaces*, 2014, **6**, 9913–9919.
15 R. A. Street, D. Davies, P. P. Khlyabich, B. Burkhart and B. C. Thompson, *J. Am. Chem. Soc.*, 2013, **135**, 986–989.
16 P. P. Khlyabich, A. E. Rudenko, B. C. Thompson and Y. L. Loo, *Adv. Funct. Mater.*, 2015, **25**, 5557–5563.
17 H. Li, Z.-G. Zhang, Y. Li and J. Wang, *Appl. Phys. Lett.*, 2012, **101**, 163302.
18 Y. Yang, W. Chen, L. Dou, W.-H. Chang, H.-S. Duan, B. Bob, G. Li and Y. Yang, *Nat. Photonics*, 2015, **9**, 190–198.
19 J. Mai, T.-K. Lau, J. Li, S.-H. Peng, C.-S. Hsu, U.-S. Jeng, J. Zeng, N. Zhao, X. Xiao and X. Lu, *Chem. Mater.*, 2016, **28**, 6186–6195.
20 Y. H. Chao, J. F. Jheng, J. S. Wu, K. Y. Wu, H. H. Peng, M. C. Tsai, C. L. Wang, Y. N. Hsiao, C. L. Wang, C. Y. Lin and C. S. Hsu, *Adv. Mater.*, 2014, **26**, 5205–5210.
21 H. Zhou, Y. Zhang, J. Seifter, S. D. Collins, C. Luo, G. C. Bazan, T. Q. Nguyen and A. J. Heeger, *Adv. Mater.*, 2013, **25**, 1646–1652.
22 U. S. Jeng, C. H. Su, C.-J. Su, K.-F. Liao, W.-T. Chuang, Y.-H. Lai, J.-W. Chang, Y.-J. Chen, Y.-S. Huang, M.-T. Lee, K.-L. Yu, J.-M. Lin, D.-G. Liu, C.-F. Chang, C.-Y. Liu, C.-H. Chang and K. S. Liang, *J. Appl. Crystallogr.*, 2010, **43**, 110–121.
23 T. Liu, L. Huo, X. Sun, B. Fan, Y. Cai, T. Kim, J. Y. Kim, H. Choi and Y. Sun, *Adv. Energy Mater.*, 2016, **6**, 1502109.
24 L. Lu, W. Chen, T. Xu and L. Yu, *Nat. Commun.*, 2015, **6**, 7327.
25 W. Chen, M. P. Nikiforov and S. B. Darling, *Energy Environ. Sci.*, 2012, **5**, 8045–8074.
26 X. Lu, H. Hlaing, D. S. Germack, J. Peet, W. H. Jo, D. Andrienko, K. Kremer and B. M. Ocko, *Nat. Commun.*, 2012, **3**, 795.
27 R. D. Deegan, O. Bakajin, T. F. Dupont, G. Huber, S. R. Nagel and T. A. Witten, *Nature*, 1997, **389**, 827–829.
28 H.-C. Liao, C.-S. Tsao, Y.-T. Shao, S.-Y. Chang, Y.-C. Huang, C.-M. Chuang, T.-H. Lin, C.-Y. Chen, C.-J. Su, U. S. Jeng, Y.-F. Chen and W.-F. Su, *Energy Environ. Sci.*, 2013, **6**, 1938–1948.
29 S. H. Liao, H. J. Jhuo, Y. S. Cheng and S. A. Chen, *Adv. Mater.*, 2013, **25**, 4766–4771.
30 J. D. Chen, C. Cui, Y. Q. Li, L. Zhou, Q. D. Ou, C. Li, Y. Li and J. X. Tang, *Adv. Mater.*, 2015, **27**, 1035–1041.
31 L. Luyao, X. Tao, C. Wei, S. L. Erik and Y. Luping, *Nat. Photonics*, 2014, **8**, 716–722.
32 V. Shrotriya, Y. Yao, G. Li and Y. Yang, *Appl. Phys. Lett.*, 2006, **89**, 063505.
33 X. Guo, N. Zhou, S. J. Lou, J. Smith, D. B. Tice, J. W. Hennek, R. P. Ortiz, J. T. L. Navarrete, S. Li, J. Strzalka, L. X. Chen, R. P. H. Chang, A. Facchetti and T. J. Marks, *Nat. Photonics*, 2013, **7**, 825–833.
34 B. Qi and J. Wang, *Phys. Chem. Chem. Phys.*, 2013, **15**, 8972–8982.